Journal of
Polymer Materials

Tech Science Press

DOI: 10.32604/jpm.2024.054660

ARTICLE

Synthesis and Characterization of Photothermal Responded Chitosan/Nanodiamond-Based Composite Beads with Enhanced Control Release Properties

Yu Luo[1,2,3], Mengna Zong[1,2,3], Jin Wang[1,2,3], Xuechun Wang[1,2,3], Bo Bai[1,2,3,*], Chunyu Zhou[1,2,3,*], Junlin Zhu[1,2,3], Jianyu Xing[1,2,3] and Moses M. C. Carlon Jr[1,2,3]

[1]School of Water and Environment, Chang'an University, Xi'an, 710054, China

[2]Key Laboratory of Subsurface Hydrology and Ecological Effect in Arid Region of the Ministry of Education, Chang'an University, Xi'an, 710054, China

[3]Key Laboratory of Eco-Hydrology and Water Security in Arid and Semi-Arid Regions of Ministry of Water Resources, Chang'an University, Xi'an, 710054, China

*Corresponding Authors: Bo Bai. Email: baibochina@163.com; Chunyu Zhou. Email: zhouchy@chd.edu.cn

Received: 04 June 2024 Accepted: 15 July 2024 Published: 09 August 2024

ABSTRACT

In this research, we developed a novel photo-stimulation-responsive composite sphere with a semi-interpenetrating polymer network (semi-IPN) structure, synthesized via an alkali gel method, to enhance the efficiency of agrochemicals. Chitosan (CS) serves as the structural matrix and protective shell, with a loading capacity for the plant growth hormone indole-3-butyric acid (IBA) of up to 41.73 μg/mg, effectively controlling the abrupt release of auxin. The incorporation of photothermal detonation nanodiamond (DND) and the photosensitive poly(N-isopropylacrylamide) (PNIPAm) endows the spheres with the ability to respond to light and temperature stimuli, achieving intelligent control over IBA release. Characterization of the composite spheres was performed using scanning electron microscopy (SEM), Fourier-transform infrared spectroscopy (FT-IR), and thermogravimetric analysis (TGA). Detailed discussions on the photothermal conversion and controlled release properties of the beads unveiled a novel mechanism by which photothermal reactions control drug release. At elevated temperatures, the cumulative release rate of IBA notably increased to 40.4%. Furthermore, pea growth under xenon lamp-simulated sunlight demonstrated significant enhancements in root (2.86 cm) and stem (2.19 cm) length following the application of the system. This study presents an innovative approach for modern agriculture, with promising implications for precision farming and environmental conservation.

KEYWORDS

Nanodiamond; photothermal conversion; controlled-release; auxin; indole-3-butyric acid

1 Introduction

In recent years, the relentless growth of the global population has led to a dire world food situation. Rational use of pesticides can significantly enhance crop yield and quality; however, less

than 1% of traditional pesticides remain on target. This inefficient pesticide application not only causes extensive ecological damage but also results in significant environmental pollution [1,2]. To mitigate environmental harm and boost the efficiency of pesticide use, there has been a shift towards intelligent controlled release systems for natural polymer-based pesticides. These systems allow the carrier to respond to environmental stimuli (pH [3], temperature [4], enzymes [5] and light [6]), thereby extending the application cycle, reducing pesticide quantities, and improving overall efficiency [7].

Synthetic polymer materials, known for their environmental responsiveness, high absorption, and other characteristics, are often employed for the controlled release of agricultural active substances. The most prevalent synthetic material is the temperature-sensitive poly(N-isopropylacrylamide) (PNIPAm), which has a lower critical solution temperature (LCST) of 32°C. Above this temperature, PNIPAm undergoes a reversible phase transition in water, shifting from an extended random coil to a dense spherical conformation [8]. Thus, thermal stimulation can alter the hydrophobicity of PNIPAm and regulate the release of active ingredients. In recent years, thermosensitive polymers like PNIPAm have been widely used in drug-controlled release, chemical sensing, and biochemical separation [9]. However, the practical application of maintaining medium temperatures over long periods is unfeasible, necessitating the introduction of a photothermal agent capable of absorbing light energy and converting it into heat energy [10].

Liu et al. [11] synthesized a nanocomposite hydrogel with significant near-infrared thermal conversion capability by embedding PDA@CNC in a thermally responsive PNIPAm network, enabling remote control of 5-fluorouracil release using a near-infrared laser. Similarly, de Solorzano et al. [12] have developed a hybrid hydrogel that integrates PNIPAm with magnetite, a material known for its photothermal conversion properties. Magnetite nanoparticles (MNPs), when dispersed within the hydrogel, can absorb visible light and transform it into heat energy. This conversion heats the hydrogel matrix, triggering a volume shrinkage in response to temperature fluctuations. Despite these advancements, current photothermal materials, such as PDA and magnetite nanoparticles, face challenges including low photothermal conversion efficiency and poor biocompatibility. Therefore, it is crucial to develop photothermal conversion materials with excellent biocompatibility, high thermal conductivity, and surface functionality. Compared to PDA and nano- magnetite, detonation nanodiamond (DND), which is formed by an SP^3-carbon diamond core and a reconstructed SP^2-carbon surface layer, is an even more ideal photothermal absorbing material. The outer surface of DNDs is rich in chemically active groups such as carboxyl, hydroxyl, carbonyl, nitrogen, and sulfur, facilitating its integration into hydrogels for photo-responsive controlled release performance [13–15].

Meantime, Chitosan (CS) is a polycationic linear polysaccharide composed of n-acetylglucosamine and D-glucose residues arranged in a β-1,4-glucan chain. It is biocompatible, biodegradable, hydrophilic, and exhibits remarkable gel properties in the presence of bivalent cations [16,17]. Building on this research, CS, PNIPAm, DND, and indole butyrate (IBA) were used as raw materials to design and prepare a novel photothermal responsive composite material. This material offers the benefits of slowing drug release, prolonging drug action time, and reducing environmental pollution. PNIPAm and DND are encapsulated within a CS polymer matrix through van der Waals forces and hydrogen bond interactions, forming a semi-interpenetrating network structure. The synergistic action of the thermosensitive polymer PNIPAm and the photothermal agent DND can control the release of plant auxins under photothermal conditions. In this study, controlled-release properties of the samples under light and heat were thoroughly investigated, along with its impact on pea growth. The application of this composite material offers a simple and efficient method for controlled release of IBA and holds promising prospects for intelligent responsive controlled release systems. The methodology for the preparation of chitosan/nanodiamond-based composite beads is represented in Fig. 1.

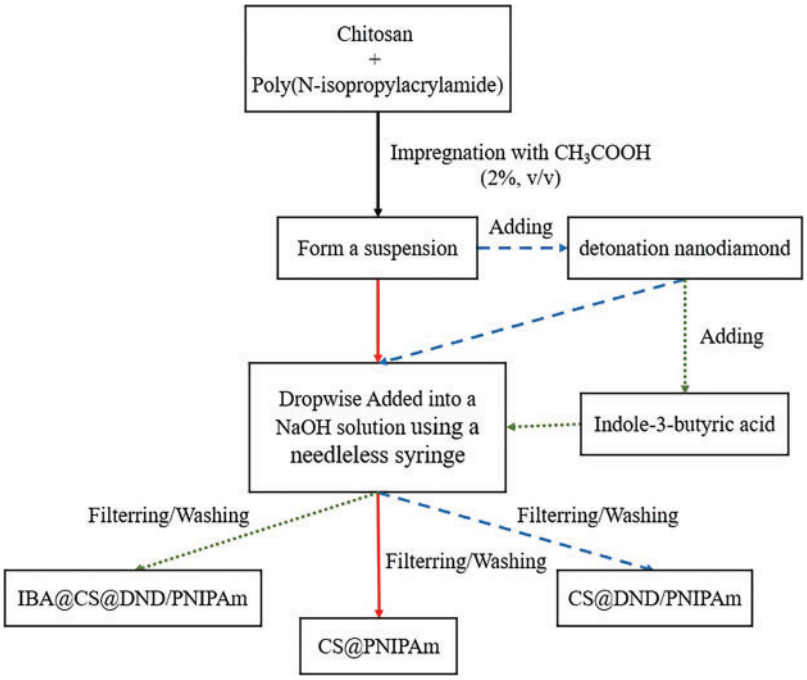

Figure 1: Methodology for preparation of chitosan/nanodiamond-based composite beads

2 Experimental

2.1 Materials

Nanodiamonds were prepared using detonation method by Yilin Inc. (Shaanxi, China). Chitosan (CA, deacetylation degree ≥90% and viscosity average molecular weight of 70–80 kD) was bought from Sinopharm Chemical Reagent Co., Ltd. (Shanghai, China). NIPAm was purchased from Sigma-Aldrich Trade Co., Ltd. (Shanghai, China). N, N, N′, N′-Tetramethylethylenediamine was afforded by Shanghai Macklin Biochemical Co., Ltd. (Shanghai, China). Indole-3-butyric acid (IBA) was provided by Shanghai Jinsui Bio-Technology Co., Ltd. (Shanghai, China). Glacial acetic acid, sodium hydroxide (NaOH), etc., were provided by Shanghai Aladdin Biochemical Technology Co., Ltd. (Shanghai, China). The reagents used were all analytical grade. Deionized water was used during sample preparation.

2.2 Instruments

Fourier transform infrared spectrometer (FT-IR, TENSOR-27), cold field emission scanning electron microscopy (SEM, Hitachi S-4800), and ultraviolet-visible diffuse reflectance spectroscopy (UV-vis, UV-3600i Plus) were used to characterize the functional groups, surface morphology, and light absorption properties of the samples, respectively. Thermogravimetric analysis (TGA) curves were obtained using a thermogravimetric analyzer (HCT-3). Zeta potential was measured by ZEN3700.

2.3 Preparation of CS@ PNIPAm and Its Lower Critical Solution Temperature Analysis

2.3.1 Preparation of Linear PNIPAm

The NIPAM monomer (0.2 g) was dissolved in 5 mL of deionized water under a nitrogen atmosphere, employing constant stirring to ensure complete dissolution. Subsequently, 5 mg of potassium persulfate and 5 μL of N, N, N′, N′-Tetramethylethylenediamine were precisely added to

the reaction mixture. The mixture was then allowed to react under a nitrogen atmosphere (N_2) for 10 min, after which it was left to dry for a period of 24 h. This process resulted in the formation of the desired linear poly(N-isopropylacrylamide) (PNIPAm).

2.3.2 Preparation of CS@PNIPAm

A suspension was prepared by blending one part of the PNIPAm with 0.4 g of chitosan in a 20 mL solution of acetic acid (2%, v/v). Following this, the mixture was left to stand to facilitate the escape of air bubbles. Subsequently, it was gently dispensed into a 2 mol/L sodium hydroxide (NaOH) solution using a paste dropper, allowing the formation of gel beads. These beads were cured at ambient temperature, then filtered and rinsed with deionized water to yield the final chitosan/PNIPAm composite product, denoted as CS@PNIPAm.

2.3.3 Lower Critical Solution Temperature Analysis of CS@PNIPAm

Thermal stimulation influences the balance of surface hydrophilicity and hydrophobicity, which in turn affects the transmittance of the material [6]. The lower critical solution temperature (LCST) of PNIPAm was investigated, aiming to analyze how the transmittance of the polymer solution varies with temperature using UV-vis spectroscopy. An aqueous solution of PNIPAm was prepared at a specific concentration, and its transmittance was measured using a 752N UV-vis spectrophotometer equipped with a thermostatic water bath. The spectrophotometer was set to the maximum absorption wavelength, and the sample was heated incrementally from 20°C to 35°C. By examining the transmittance *vs*. temperature curve, the LCST of the polymer compound was determined. All experiments were conducted in triplicate.

2.4 Preparation of CS@DND/PNIPAm and Determination of Its Photothermal Conversion

2.4.1 Preparation of CS@DND/PNIPAm

0.4 g of chitosan was introduced into a 20 mL solution of acetic acid (2%, v/v) and stirred vigorously to ensure complete dissolution. Thereafter, a calculated quantity of PNIPAm and 0.04 g of detonation nanodiamond (DND) were incrementally incorporated into the mixture, forming a suspension with a DND concentration of 2 mg/mL. Following thorough agitation and a period of settling to eliminate air bubbles, the mixture was extruded into a 2 mol/L NaOH solution using a needleless syringe, thereby forming gel beads. The nascent beads were subsequently cured at room temperature, subjected to filtration through a metal sieve, and rinsed to produce the CS@DND/PNIPAm composite.

2.4.2 Determination of Photothermal Conversion of CS@DND/PNIPAm

The photothermal conversion properties of DND, CS@PNIPAm, and the CS@DND/PNIPAm composite beads were characterized using UV-vis near-infrared diffuse reflectance spectroscopy. The impact of DND on the photothermal conversion ability of CS@PNIPAm beads was assessed by measuring the photothermal effects of CS@DND/PNIPAm aqueous solutions with varying DND concentrations and the composite beads under different light intensities. Initially, the CS@DND/PNIPAm aqueous solution with different DND concentrations and a control (equal volume of deionized water) were exposed to xenon lamp irradiation at 100 mW/cm^2 for 10 min. The temperature changes of the solutions at fixed time points were monitored using an infrared thermal camera. Additionally, the temperature changes of the CS@DND/PNIPAm composite beads were measured after 10 min of illumination at varying light intensities (50, 75, 100, 125, 150 mW/cm^2).

Finally, the photothermal stability of the CS@DND/PNIPAm composite beads was evaluated. The CS@DND/PNIPAm solution was subjected to irradiation under a 100 mW/cm^2 Xenon lamp for

approximately 10 min, during which the temperature change was monitored and recorded. Following this initial phase, the solution was allowed to cool to room temperature. Once at ambient temperature, irradiation was continued for another 10 min, the temperature was recorded, and the process was repeated for a total of five cycles to assess the stability and consistency of the photothermal response.

2.5 Preparation of IBA@CS@DND/PNIPAm and Its Release Behavior

2.5.1 Preparation of IBA@CS@DND/PNIPAm

0.4 g of chitosan was incorporated into a 20 mL solution of acetic acid (2%, v/v). Subsequently, a precise amount of PNIPAm and 0.04 g of DND were sequentially added to this solution, yielding a suspension with a DND concentration of 2 mg/mL. The suspension was then homogeneously mixed with an indole-3-butyric acid (IBA) solution to form a uniform mixture. After thorough stirring and a period of settling to remove air bubbles, gel beads were formed by extruding the mixture into a 2 mol/L NaOH solution using a needleless syringe. The beads were cured at room temperature, filtered through a metal sieve, and washed to obtain the final product, designated as IBA@CS@DND/PNIPAm.

2.5.2 Release Behavior of IBA

To ascertain the thermal-responsive slow-release characteristics of the composite beads, a defined quantity was immersed in deionized water (15 mL) at temperatures of 20°C, 25°C, and 40°C, respectively. At predetermined time intervals, 3 mL aliquots of the release medium were extracted and analyzed using UV-vis spectroscopy at the maximum absorption wavelength of 281 nm, while an equivalent volume of deionized water was replenished to maintain the system. Additionally, for assessing the light-responsive release of IBA, a specific quantity of the composite beads was placed in 10 mL of deionized water. These were then exposed to a light intensity of 100 mW/cm^2 for 2 h at various time intervals. The concentration of IBA in the solution was measured using a UV-vis spectrophotometer; 3 mL samples were taken at regular intervals, and the solution was immediately replenished with an equal volume of deionized water. All data are the average of at least three determinations. Ultimately, the cumulative release percentage (RP) [18] of IBA was calculated using the following formula:

$$\mathrm{RP}\,(\%) = \frac{15\mathrm{C_t} + \sum_0^{t-1} \mathrm{C_t V_t}}{\mathrm{m_0}} \times 100\% \tag{1}$$

where $\mathrm{m_0}$ (μg) represents the IBA content of CS@DND/PNIPAm beads before release, and $\mathrm{C_t}$ (μg/mL) and $\mathrm{V_t}$ (mL) are the IBA concentration and volume of the extract at time t.

2.5.3 Release Kinetics

In this paper, the release kinetics of CS@DND/PNIPAm beads were investigated with the primary model, Korsmeyer-Peppas, and Higuchi [19,20].

$$\ln\left(1 - \frac{M_t}{M_\infty}\right) = -kt \tag{2}$$

$$\frac{M_t}{M_\infty} = kt^n \tag{3}$$

$$\frac{M_t}{M_\infty} = kt^{0.5} + \mathrm{b}t \tag{4}$$

where M_t and M_∞ denote the cumulative release of the drug at the moment of time t and when equilibrium is reached, respectively, in μg/mL; k is the release kinetic constant of the spheroid system; b is a constant; and n is the release index that characterizes the release mechanism.

2.6 Application Evaluation

In this research, the performance of IBA-loaded semi-IPN CS@DND/PNIPAm composite beads in the photo-controlled release of IBA was evaluated through rooting and germination experiments on peas. Uniform-sized, undamaged pea seeds were immersed for 9 h in solutions containing varying concentrations (26, 260, or 520 mg/L) of CS@DND/PNIPAm, as well as in pure water as a control. Concurrently, a separate group of pea seeds was soaked in a 26 mg/L CS@DND/PNIPAm solution, with xenon lamp illumination applied twice during the soaking period, each lasting 30 min. Following the soaking process, all seeds were rinsed with distilled water and then arranged on petri dishes lined with moistened filter paper. Each dish contained ten pre-soaked pea seeds, and the filter paper was consistently kept damp with water. Measurements of both root and shoot length were recorded at intervals of 0, 1, 3, 5, and 7 days post-soaking, with the average values being documented for analysis. All experiments were conducted in triplicate.

3 Results and Discussion

3.1 Preparation Mechanism of CS@DND/PNIPAm Beads

To augment the efficacy and precision of pesticide application, we have developed innovative photothermal-sensitive beads designated as CS@DND/PNIPAm. These beads are engineered for the intelligent controlled release of agrochemicals. The chitosan (CS) matrix within the beads structure is distinguished by its exceptional biodegradability and biocompatibility [21]. Embedded within this matrix is poly(N-isopropylacrylamide) (PNIPAm), a temperature-responsive polymer that exhibits a reversible phase transition at 32°C, shifting from an irregular coil to a compact spherical conformation [22]. The integration of detonation nanodiamond (DND) as a photothermal agent endows the beads with superior light absorption and thermal conductivity, facilitating the conversion of light energy into heat and the subsequent activation of temperature-sensitive monomers for drug release [23]. The mechanisms underlying the formation of these composite beads and the release of their pharmaceutical payloads are delineated in Fig. 2.

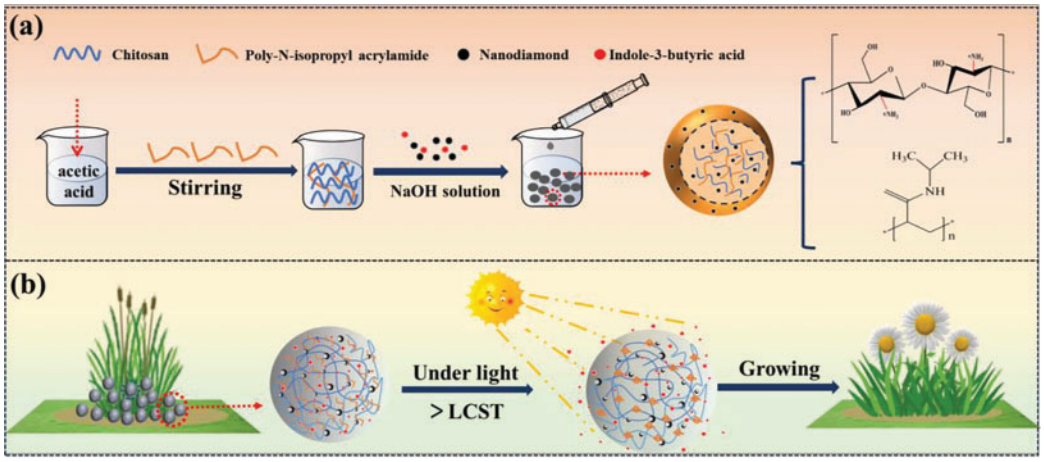

Figure 2: Proposed schematic diagram. (a) The synthetic process of the IBA@CS@DND/PNIPAm bead, and (b) its light-responsively controlled-release performance

In this study, PNIPAm and DND were integrated into the CS suspension through hydrogen bonding, ensuring that the gel network structure remains intact under photothermal stimuli. Initially, CS was dissolved in a 2% acetic acid solution. After thorough stirring, the -NH_2 groups within CS reacted with the acid, leading to the formation of -NH_3^+. Simultaneously, the hydroxyl groups in CS interacted with N-acetylamide to form intramolecular hydrogen bonds. The entanglement of CS molecules, driven by van der Waals forces and hydrogen bonding, resulted in a three-dimensional network structure [24]. Subsequently, the temperature-sensitive polymer PNIPAm was incorporated into this structure. The electrostatic repulsion of the -NH_3^+ groups ensured a uniform distribution of PNIPAm within the CS network. The addition of DND nanoparticles marked a critical juncture, as their -OH groups engaged in hydrogen bonding with the -OH and -NH_2 groups in the CS@PNIPAm, bestowing photothermal functionality onto the composite. Ultimately, the homogeneous CS@DND/PNIPAm suspension was extruded into a NaOH solution using a syringe. Under alkaline conditions, the deprotonation of -NH_3^+ groups reduced the solubility of CS, leading to the formation of a semi-permeable cured film at the interface between the mixed solution droplet and the NaOH solution. As the film thickened through diffusion and the droplets shrank, CS@DND/PNIPAm composite beads were successfully formed.

3.2 Lower Critical Solution Temperature Analysis of CS@PNIPAm

The turbidity test was utilized to monitor the solubility changes of CS and CS@PNIPAm to research the thermal response behaviors of samples. Fig. 3a,b demonstrate the relationship between temperature and transmittance, where the inflection point corresponds to the lower critical solution temperature (LCST) [25]. At lower temperatures, CS@PNIPAm mirrors the transparency of CS. However, upon an increase in temperature, the molecular chains of the composite material contract significantly, by a factor of eight, leading to the solution's opacity. As a result, the phase transition temperature for CS@PNIPAm is identified as 33°C. This lower LCST is beneficial for the controlled release of plant auxins under light exposure.

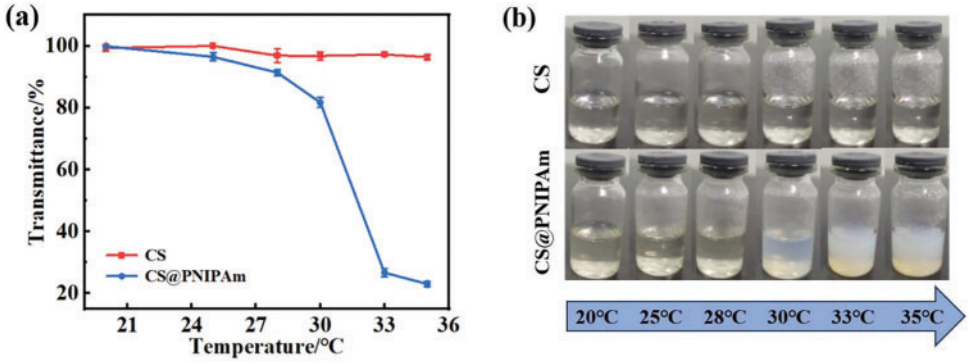

Figure 3: LCST determination under the conditions: pH = 6. (a) Transmittance of samples at different temperatures, (b) corresponding photographs of samples

3.3 Photothermal Conversion of CS@DND/PNIPAm Beads

Photothermal materials are capable of transforming absorbed solar energy into thermal energy. Notably, carbon-based materials capitalize on the superior light-absorbing capabilities of ferrous materials to effect photothermal conversion. The light absorption characteristics of DND, CS@PNIPAm and CS@DND/PNIPAm beads were evaluated using UV-vis diffuse reflectance spectroscopy, with the outcomes depicted in Fig. 4a. The CS@PNIPAm beads demonstrated a restricted capacity for light absorption across the visible and infrared spectrum. In stark contrast, the DND, known for

its photothermal properties, exhibited pronounced absorbance across the entire UV-vis-NIR range (250–2500 nm). This broad absorption spectrum underscores DND's superior light-trapping ability, a trait that is conducive to efficient photothermal conversion. Furthermore, upon incorporating DND into CS@PNIPAm, the resulting CS@DND/PNIPAm composite beads with augmented light absorption across the full spectral range. This finding underscores the incorporation of DND into CS@DND/PNIPAm beads, endowing them with broader and more intense absorption capabilities. The enhanced light absorption of the CS@DND/PNIPAm composite beads represents a strategic advancement, poised to elevate photothermal conversion efficiency, thereby facilitating the controlled release of agrochemicals or plant growth regulators in a stimulus-responsive manner.

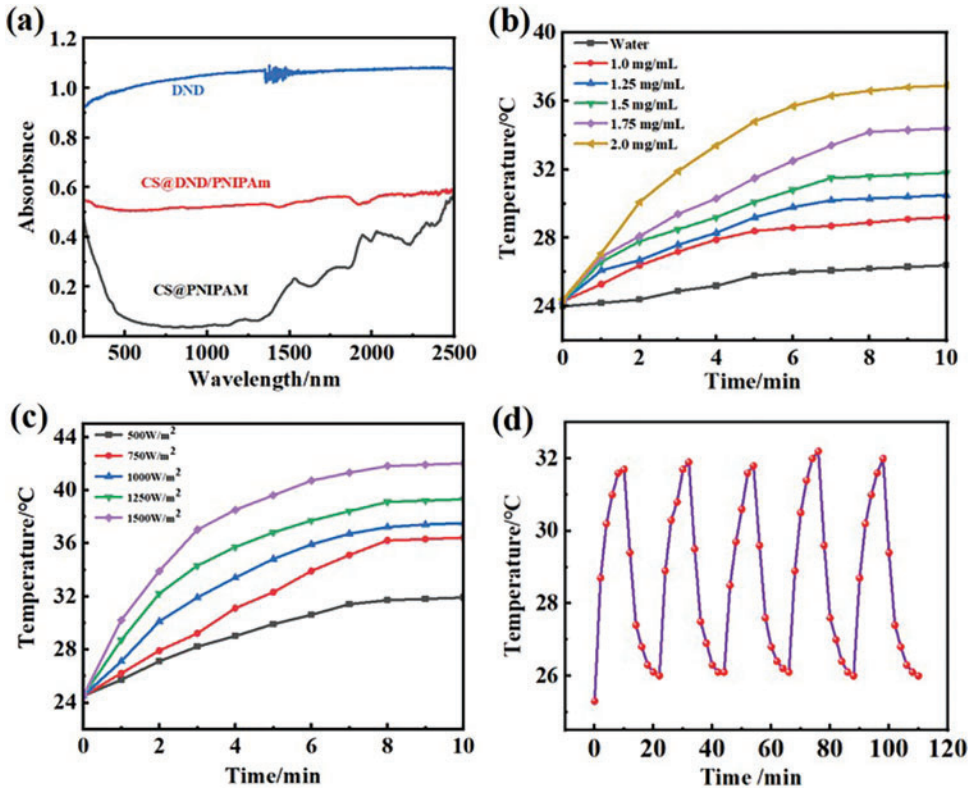

Figure 4: Performance of CS@DND/PNIPAm beads. (a) UV-vis diffuse reflectance spectra of CS@PNIPAm, DND, and CS@DND/PNIPAm beads; (b) The temperature change with time of different concentrations of DND under one light intensities for 10 min; (c) Temperature profiles of CS@DND/PNIPAm beads under different light intensities; (d) Photothermal stability of CS@DND/PNIPAm aqueous solution

The photothermal conversion capabilities of the CS@DND/PNIPAm composite beads were evaluated under varying concentrations and irradiation intensities. As depicted in Fig. 4b, after 10 min of exposure to light, the temperature incrementally stabilized, with the highest recorded increase being 12.5°C, indicative of DND's commendable photothermal conversion efficiency. The marked elevation in temperature corroborates the exceptional photothermal conversion prowess of the composite beads. Furthermore, the temperature dynamics within the CS@DND/PNIPAm aqueous solution, under a gradient of light intensities (50 to 150 mW/cm^2), were meticulously tracked, as illustrated in Fig. 4c. These observations accentuate the beads' acute sensitivity and adaptive response to fluctuating irradiation conditions, indicative of their potential in tunable photothermal applications. In pursuit of assessing the durability of photothermal conversion, the CS@DND/PNIPAm composite beads were

subjected to a regimen of intermittent illumination. The outcomes, delineated in Fig. 4d, reveal that the beads sustained their photothermal conversion efficacy across five cycles of light exposure and intermission. This steadfast performance exemplifies their robust photothermal stability, a coveted attribute for sustainable use in responsive drug delivery systems. These findings not only affirm the DND's robust photothermal characteristics but also spotlight the pioneering integration of DND within the CS@DND/PNIPAm composite beads. This strategic integration represents a notable stride, affirming the beads as a potent photothermal agent.

3.4 Interaction Analyses

Firstly, the thermal stability of the beads was investigated by TGA, with the findings [26] are shown in Fig. 5a. DND exhibited excellent thermal stability, with a minimal mass loss of about 10% occurring below 500°C. However, within the high -temperature range of 500°C–750°C, a significant mass loss was observed due to carbon epoxidation. The thermal degradation of PNIPAm occurred in two distinct phases. During the initial phase (170°C–340°C), a 5% mass loss was attributed to the cleavage of the side chains and cross-linked segments of the PNIPAm polymer matrix. In the subsequent phase (340°C–600°C), a more substantial mass loss of 54.5% was p rimarily due to the degradation of the polymer backbone at elevated temperatures. In stark contrast, the CS@DND/PNIPAm composites exhibited two significant mass loss events within similar temperature ranges. The composite experienced one mass loss in the same temperature range as DND (600°C–750°C), signifying the oxidation of carbon rings. This finding su ggests that DND contributed to the mass loss within this temperature range. Additionally, another notable mass loss in the composite was detected between 200°C and 500°C, corresponding to the oxidative decomposition of PNIPAm, thereby affirming the polymer's role in the composite's mass reduction during this temperature span. This study conducted a detailed thermal characterization of the CS@DND/PNIPAm composite system, elucidating the individual and collective thermal behaviors of its components.

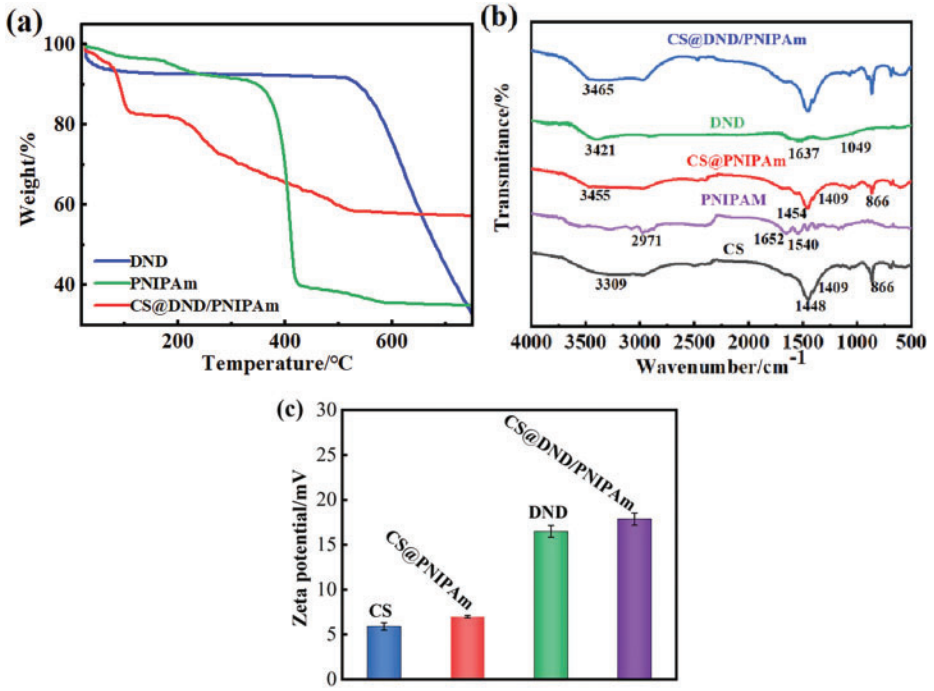

Figure 5: Illustrative analysis of interaction within the CS@DND/PNIPAm beads. (a) TGA curve; (b) FT- IR spectra and (c) Zeta potential of samples

The interactions within the samples were characterized using FT-IR spectrometry, which also confirmed the successful preparation of the IBA@CS@DND/PNIPAm composite beads. As depicted in Fig. 5b, the characteristic peaks for CS are found at 866 and 3309 cm^{-1}, corresponding to the C-O stretching vibration along the backbone [27] and the stretching vibration of -OH and -N-H within the $-NH_2$ [28], respectively. Similarly, the peaks at 1448 and 1409 cm^{-1} are indexed to the bending vibrations of $-NH_2$ and -OH, respectively [29]. The distinctive peaks for PNIPAm appear at 2971, 1652, and 1540 cm^{-1}, corresponding to the asymmetric stretching vibration of the $-CH_3$ group, the stretching vibration of the secondary amide C=O, and the deformation vibration of the secondary amide N-H, respectively. These results are in line with previous studies on PNIPAm [30]. The absorption peaks of the CS@PNIPAm beads align with those of their constituent monomers, indicating that the beads contain both chitosan derivatives and PNIPAm. The characteristic absorption peaks of DND are observed at 3421, 1637, and 1049 cm^{-1}, which are associated with the stretching and bending vibrations of -OH groups and the C-C stretching vibration of the graphite structure, respectively. This suggests that DND is rich in -OH functional groups and C-C bonds [31,32]. The shift in the stretching vibration peak from 3455 cm^{-1} for CS@PNIPAm to 3465 cm^{-1} for CS@DND/PNIPAm further confirms that DND and CS@PNIPAm are combined through hydrogen bonding. Collectively, these findings substantiate the successful fabrication of the composite beads. The detailed spectral analysis reveals the synergistic integration of DND's hydroxyl-rich surface with the PNIPAm and CS matrix.

To assess the surface characteristics of CS@DND/PNIPAm, zeta potential analysis was conducted, yielding critical insights into the colloidal stability and defining features of the surface charge. As depicted in Fig. 5c, the average surface charge of CS is 5.90 mV. Given that PNIPAm's molecular structure typically lacks a charge, the elevated zeta potential observed in CS@PNIPAm, at 7.00 mV, implies a successful interfacial integration with CS, potentially through subtle charge transfer or altered hydration effects at the surface. Furthermore, the CS@DND/PNIPAm composite beads, formed by blending CS@PNIPAm with the positively charged DND, exhibit an even higher zeta potential of 17.85 mV, likely due to the DND's contribution of additional positive charges, stemming from their abundant hydroxyl groups capable of ionization. This finding effectively confirms the successful amalgamation of CS@PNIPAm with DND.

3.5 Morphology Observation

The morphology of the materials was characterized using macroscopic maps and an SEM. It can be seen from Fig. 6h that the three types of beads prepared had diameters ranging from 3–4 mm. The color of the chitosan (CS) and CS@PNIPAm beads progressively intensified, shifting from translucent to an opaque white. The black coloration of the CS@DND/PNIPAm beads signified the successful incorporation of detonation nanodiamond (DND). Upon drying, there was a noticeable reduction in size by 1–2 mm for all beads. Subsequently, the samples were observed under SEM magnification. As depicted in Fig. 6a–c), the surfaces of the CS, CS@PNIPAm, and CS@DND/PNIPAm samples exhibited irregularities. Cross-sectional analysis revealed that the pure CS beads possessed a relatively smooth morphology (Fig. 6d). In contrast, the CS@PNIPAm beads exhibited distinct laminar folds (Fig. 6e), a feature attributed to the layered structure of PNIPAm (Fig. 6f). The CS@DND/PNIPAm beads displayed a cross-sectional morphology akin to that of the CS@PNIPAm (Fig. 6g), suggesting a conserved structural integrity post-DND integration. Moreover, as depicted in Fig. 6i,j, Energy-Dispersive X-ray Spectroscopy (EDS) analysis of the CS@PNIPAm and CS@DND/PNIPAm samples indicated an increase in carbon content from 52.5% to 61.3%, further confirming the successful integration of DND into the CS@PNIPAm composite. This increase in carbon signature is attributed to the DND's carbonaceous composition, thereby confirming its integration into the composite matrix.

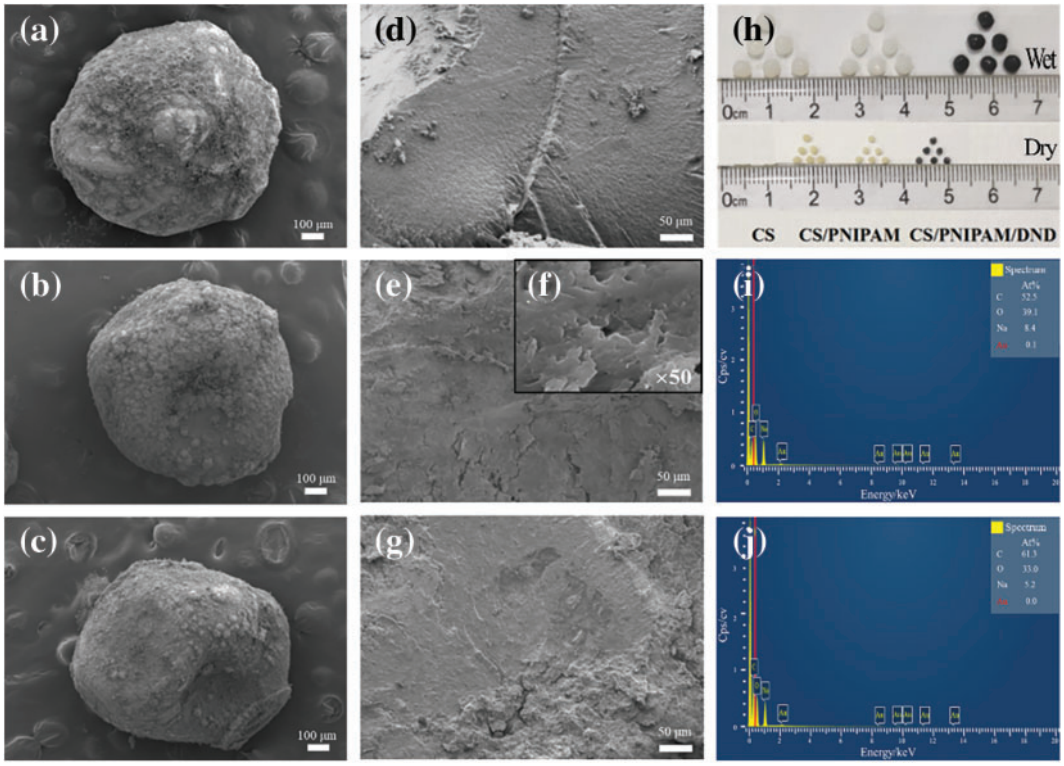

Figure 6: Analysis of beads surface morphology. SEM image of (a, d) CS beads; (b, e) CS@PNIPAm beads; (f) PNIPAm; (c, g) CS@DND/PNIPAm beads; (h) Pictures of beads; EDS diagram of (i) CS@PNIPAm and (j) CS@DND/PNIPAm

3.6 Controlled Release Behavior of Indole-3-Butyric Acid

Indole-3-butyric acid (IBA) serves as a plant growth regulator, known for its ability to enhance seed germination as well as the growth and development of plant vegetative organs. Owing to its efficacy, IBA has been widely adopted in contemporary agricultural practices [33]. Consequently, IBA was selected as the model auxin for this study. Based on our calculations, the CS@DND/PNIPAm beads demonstrated an IBA loading capacity of 41.73 μg/mg.

3.6.1 Temperature-Responsive Release of IBA and Related Mechanism

The release of IBA from CS@DND/PNIPAm was examined across a range of temperatures. According to Fig. 7a, the rate at which IBA was released from the composite beads escalated with rising temperature. The cumulative release rate of IBA increased from 14.6% at 20°C to 18.4% at 25°C, predominantly driven by water absorption and the hydrophilic nature of the composite at lower temperatures. This rate further escalated to 40.4% at 40°C, a result of the incorporation of PNIPAm, a temperature-sensitive component that bestows the composite beads with a unique Lower critical solution temperature (LCST). Below the LCST, PNIPAm remains soluble, inducing a porous structure in the composite spheroids, facilitating the gradual diffusion of IBA into the surrounding solution as water molecules permeate the matrix. Conversely, when the temperature exceeds the LCST, the hydrophobic methyl groups of PNIPAm become exposed and contract, forming a heat-sensitive chain. This temperature-induced phase transition results in the formation of a heat-responsive scaffold, concurrently creating numerous pores on the surface of the composite beads. This pore formation enhances the liberation of IBA molecules from the composite matrix through these channels.

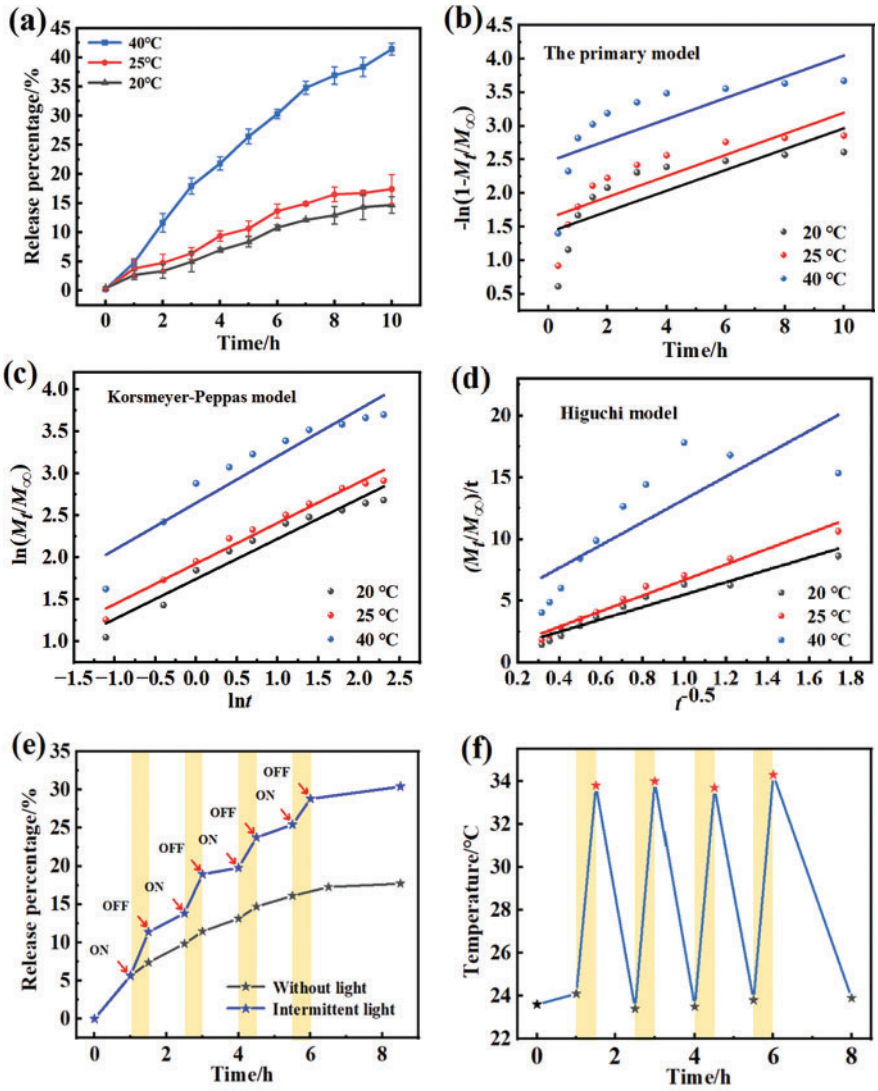

Figure 7: Elucidating the mechanisms of photothermal-induced IBA delivery. (a) Release profiles of IBA under different temperatures (20°C, 25°C, and 40°C) in deionized water; (b) The primary model; (c) Korsmeyer–Peppas model; (d) Higuchi model; (e) The release of IBA from CS@DND/PNIPAm composite beads (2.0 mg/mL DND) under continuous light and non-light conditions and (f) the variation pattern with temperature

In this study, the release mechanism of IBA from the composite beads was examined using the primary model, the Korsmeyer-Peppas model and the Higuchi model [34], with the analytical results presented in Fig. 7b–d. The model selection, predicated on the correlation coefficient (R2), was discerned to ensure the most accurate representation of the release kinetics, as delineated in Table 1, the R2 values of the Korsmeyer-Peppas model were consistently higher than those of the other two models. Consequently, the Korsmeyer-Peppas model was deemed the most appropriate for fitting the experimental data. Within the Korsmeyer-Peppas model, the release index (n) is a crucial parameter for assessing the drug release mechanism from composite beads. In this research, the release index (n) of the Korsmeyer-Peppas model ranged from 0.43 to 0.89, suggesting that the release of IBA from the CS@DND/PNIPAm composite beads adhered to an anomalous diffusion pattern [35]. This finding

implicates a synergistic interplay of diffusion and polymeric matrix swelling in governing the release dynamics, underscoring the complex interdependence between the physicochemical properties of the composite and the drug release behavior. The CS@DND/PNIPAm composite beads formed a cross-linked network structure, wherein drug molecule liberation is intricately linked to the swelling kinetics and relaxation phenomena of the chitosan and PNIPAm chains. This interplay forms the cornerstone of the composite beads' ability to modulate drug release in response to environmental stimuli, offering a sophisticated strategy for controlled drug delivery.

Table 1: Parameters in different dynamics models

Temperature	The primary model		Korsmeyer–Peppas model			Higuchi model	
	K	R2	K	R2	n	K	R2
20°C	0.1548	0.6069	4.1239	0.9456	0.4782	5.0162	0.9431
25°C	0.1571	0.6879	5.0881	0.9786	0.4843	6.2925	0.9771
40°C	0.1578	0.5406	11.8248	0.8962	0.5574	9.2336	0.6728

3.6.2 Sunlight-Responsive Release Behavior and Mechanism Investigation of IBA

Photothermal-sensitive controlled release systems hold greater potential for application compared to those that are solely temperature-sensitive, as they harness the green and sustainable energy of sunlight as a direct trigger. To further validate the impact of sunlight on triggering IBA release, we conducted tests under conditions of intermittent sunlight exposure and in the complete absence of sunlight (Fig. 7e). In the absence of light, IBA was released slowly from the composite spheres via diffusion, with the cumulative release rate of IBA reaching only about 17.73% over 8.5 h. In contrast, under intermittent light, the cumulative release rate of IBA from the composite beads increased to 32.43%. The release of IBA from the CS@DND/PNIPAm composite beads was evidently dependent on light exposure (Fig. 7f). Specifically, under non-illuminated conditions (0–1 h), the medium temperature remained stable at approximately 24°C, and IBA diffusion was minimal (0%–5.67%). Upon turning on the light source (1–1.5 h), the medium temperature rose to 33.8°C, and the release rate of IBA notably increased (from 5.67% to 11.38%). When the light was turned off again (1.5–2.5 h), the medium temperature fell back to 23.4°C, and the rate of drug release decelerated (from 11.38% to 13.83%). This oscillatory release profile, continuing to subside post-illumination, affirms the enhancing effect of light exposure on drug release, predicated on the photothermal transduction mechanism. The detonation nanodiamonds (DND) dispersed within the composite beads function as efficient photothermal transducers, absorbing solar energy and converting it into heat, thereby elevating the composite beads' temperature beyond the LCST. This temperature upswing triggers a contraction of the thermo-responsive beads, accompanied by an increase in hydrostatic pressure within the gel matrix. This dynamic process propels the expulsion of the IBA-laden liquid, accelerating the release rate of IBA. The aforementioned findings confirm that the CS@DND/PNIPAm composite beads are photothermally responsive and control the release of IBA by modulating exposure to sunlight.

3.7 Practical Application Evaluation

Pea seeds were chosen as the subjects of this study to evaluate the efficacy of the IBA@CS@DND/PNIPAm composite beads on plant growth. As illustrated in Fig. 8a,b, both the root and above-ground lengths of pea seeds treated with varying concentrations of the beads (26, 260, and 520 mg/L) demonstrated an increase that correlated with the concentration of the beads. Notably, the root length

extended from 2.04 to 2.86 cm, and the shoot length grew from 1.32 to 2.19 cm, underscoring the beads' potential as a growth promoter. A comparison was made between pea seeds treated with 26 mg/L beads under conditions with and without intermittent light stimulation. It was observed that the seeds exposed to light had significantly greater root and shoot lengths than those without light exposure. This enhancement is attributed to the light-induced structural phase changes in the temperature-sensitive material within the CS@DND/PNIPAm beads, which in turn promoted the release of IBA, thereby enhancing seed rooting and germination. This study demonstrates the controlled release behavior of IBA@CS@DND/PNIPAm composite beads under solar irradiation. The CS@DND/PNIPAm composite material, with its photo-responsive characteristics, serves as a photothermal carrier for targeted and controlled release of plant auxins. This approach harnesses the natural energy of sunlight to regulate plant growth, offering sustainable and efficient applications in agriculture.

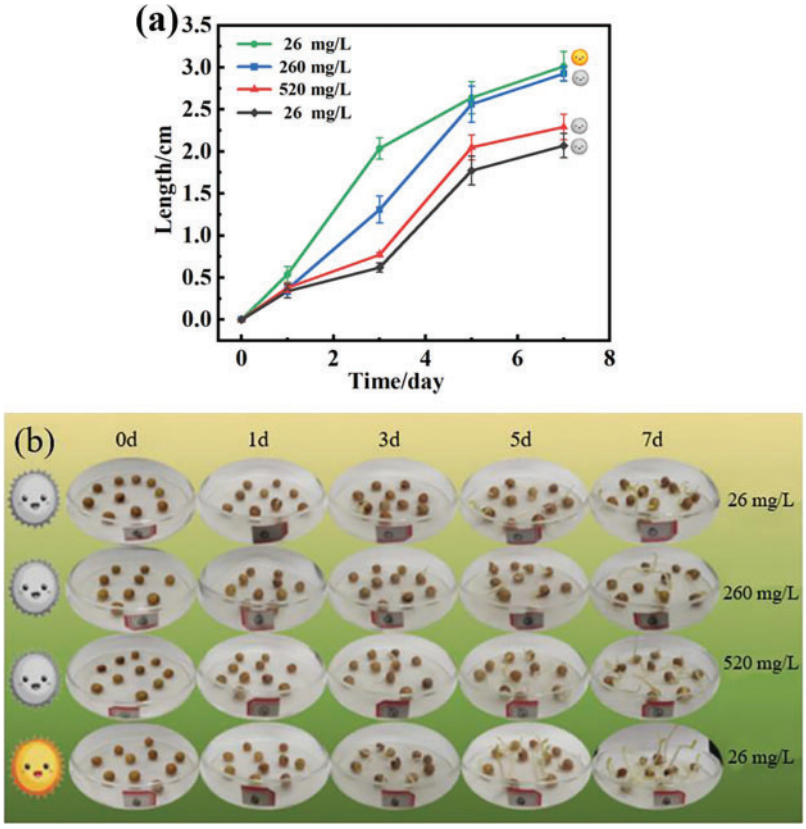

Figure 8: Efficacy of composite beads on pea seed germination and growth. (a) Data images and (b) digital images of growth of pea seeds under different treatments of light and different concentrations

4 Conclusions

In conclusion, we have designed and synthesized a promising photo-thermo-sensitive hydrogel-based controlled-release beads system, termed IBA@CS@DND/PNIPAm, utilizing CS, photosensitive DND, temperature-responsive PNIPAm, and IBA as the primary materials. The successful synthesis of these composite beads was characterized by SEM, FT-IR, TGA, and Zeta potential, and the synthesis mechanism was elucidated in detail. The results indicated that the photo-thermo conversion efficiency of the CS@DND/PNIPAm beads was contingent upon their concentration and

the irradiation power, achieving a maximum temperature increase of 12.5°C. As the temperature rose from 20°C to 40°C, the cumulative release rate of IBA from the IBA@CS@DND/PNIPAm beads increased by 25.8%. This responsive controlled-release system is capable of adjusting the release of IBA by changing the environmental conditions (light and temperature). In practical applications, the composite beads were found to enhance the growth of peas through the controlled release of IBA under photo-thermo stimulation. The photo-thermo- responsive release system developed in this study, capable of enhancing the utilization efficiency of growth regulators, demonstrates diverse application potential within the agricultural sector.

Acknowledgement: None.

Funding Statement: This work was financially supported by National Natural Science Foundation of China (No. 22202016), Scientific Research Program of Shaanxi Provincial Education Department (No. 22JE003), the High-Tech Research and Cultivation Projects for the Central Universities, CHD (No. 300102293204), National College Students' Innovative Entrepreneurial Training Plan Program, CHD (No. S202310710225), and International Education Teaching Reform Program, CHD (No. 300108231136).

Author Contributions: Yu Luo: Conceptualization; Formal analysis; Investigation; Writing—manuscript draft; Editing. Mengna Zong: Investigation; Validation; Writing—manuscript draft. Jin Wang: Investigation; Validation. Xuechun Wang: Investigation; Validation. Bo Bai: Conceptualization; Funding acquisition; Writing—review & editing; Supervision; Visualization. Chunyu Zhou: Conceptualization; Writing—review & editing; Supervision; Visualization. Junlin Zhu: Validation. Jianyu Xing: Writing—review & editing. Moses M C Carlon Jr: Validation; Writing—review & editing. All authors reviewed the results and approved the final version of the manuscript.

Availability of Data and Materials: Data supporting the findings of this study are available within the article. Additional datasets used and/or analyzed during the current study are available from the corresponding author on reasonable request.

Ethics Approval: Not applicable.

Conflicts of Interest: The authors declare that they have no conflicts of interest to report regarding the present study.

References

1. Zhao M, Zhou H, Chen L, Hao L, Chen H, Zhou X. Carboxymethyl chitosan grafted trisiloxane surfactant nanoparticles with pH sensitivity for sustained release of pesticide. Carbohydr Polym. 2020;243:116433. doi:10.1016/j.carbpol.2020.116433.
2. Xiao DX, Wu HX, Zhang YL, Kang J, Dong ALDR, Liang WL. Advances in stimuli- responsive systems for pesticides delivery: recent efforts and future outlook. J Control Release. 2022;352:288–312. doi:10.1016/j.jconrel.2022.10.028.
3. Chen H, Zhi H, Liang J, Yu M, Cui B, Zhao X, et al. Development of leaf-adhesive pesticide nanocapsules with pH-responsive release to enhance retention time on crop leaves and improve utilization efficiency. J Mater Chem B. 2021;9(3):783–92. doi:10.1039/D0TB02430A.
4. Xiao D, Liang W, Xie Z, Cheng J, Du Y, Zhao J. A temperature-responsive release cellulose-based microcapsule loaded with chlorpyrifos for sustainable pest control. J Hazard. Mater. 2021;403:123654. doi:10.1016/j.jhazmat.2020.123654.

5. Camara MC, Monteiro RA, Carvalho LB, Oliveira JL, Fraceto Enzyme LF. Stimuli–responsive nanoparticles for bioinsecticides: an emerging approach for uses in crop protection. ACS Sustain Chem Eng. 2020;9(1):106–12. doi:10.1021/acssuschemeng.0c08054.
6. Liu B, Zhang J, Chen C, Wang D, Tian G, Zhang G, et al. Infrared-light-responsive controlled-release pesticide using hollow carbon Microspheres@Polyethylene Glycol/α-cyclodextrin gel. Cyclodextrin Gel. 2021;69(25):6981–8. doi:10.1021/acs.jafc.1c01265.
7. McCarthy PC, Zhang Y, Abebe F. Recent applications of dual-stimuli responsive chitosan hydrogel nanocomposites as drug delivery tools. Molecules. 2021;26(16):4735. doi:10.3390/molecules26164735.
8. Li CA, Wang N, Jiao LY, Wang Y, Liu YP, Li XG. Safe and intelligent thermoresponsive β-cyclodextrin pyraclostrobin microcapsules for targeted pesticide release in rice disease management. ACS Appl Polymer Mater. 2024;6(3):1922–8. doi:10.1021/acsapm.3c02784.
9. Chen Z, Liu J, Chen Y, Zheng X, Liu H, Li H. Multiple-stimuli-responsive and cellulose conductive ionic hydrogel for smart wearable devices and thermal actuators. ACS Appl Mater Interfaces. 2020;13(1):1353–66. doi:10.1021/acsami.0c16719.
10. Chen T, Yang Y, Peng H, Whittaker AK, Li Y, Zhao Q, et al. Cellulose nanocrystals reinforced highly stretchable thermal-sensitive hydrogel with ultra-high drug loading. Carbohydr. Polym. 2021;266(2):118122. doi:10.1016/j.carbpol.2021.118122.
11. Liu X, Wu Y, Lin Q, Cheng J, Lin F, Tang L, et al. Polydopamine-coated cellulose nanocrystal as functional filler to fabricate nanocomposite hydrogel with controllable performance in response to near-infrared light. Cellulose. 2021;28(4):2255–71. doi:10.1007/s10570-020-03630-8.
12. de Solorzano IO, Prieto M, Mendoza G, Sebastian V, Arruebo M. Triggered drug release from hybrid thermoresponsive nanoparticles using near infrared light. Nanomedicine. 2020;15(3):219–34. doi:10.2217/nnm-2019-0270.
13. Trofimuk AD, Kirilenko DA, Kukushkina YA, Tomkovich MV, Stovpiaga EY, Kidalov EY, et al. Structure and properties of self-assembled graphene oxide-detonation nanodiamond composites. Fullerenes Nanotub Carbon Nanostruc. 2024;32(9):887–95. doi:10.1080/1536383X.2024.2340022.
14. Shang BF, Yang G, Zhang B. Phase change nanocapsules incorporated with nanodiamonds for efficient photothermal energy conversion and storage. Appl Energy. 2024;360:122806. doi:10.1016/j.apenergy.2024.122806.
15. Tamburri E, Guglielmotti V, Orlanducci S, Terranova ML, Sordi D, Passeri D, et al. Nanodiamond-mediated crystallization in fibers of PANI nanocomposites produced by template-free polymerization: conductive and thermal properties of the fibrillar networks. Polymer. 2012;53(19):4045–53. doi:10.1016/j.polymer.2012.07.014.
16. Riseh RS, Vatankhah M, Hassanisaadi M, Varma RS. A review of chitosan nanoparticles: nature's gift for transforming agriculture through smart and effective delivery mechanisms. Int J Biol Macromol. 2024;260:129522. doi:10.1016/j.ijbiomac.2024.129522.
17. Muthu M, Gopal J, Chun S, Devadoss AJP, Hasan N, Sivanesan I. Crustacean waste-derived chitosan: antioxidant properties and future perspective. Antioxidants. 2021;10(2):228. doi:10.3390/antiox10020228.
18. Zheng D, Bai B, Zhao H, Xu X, Hu N, Wang H. Stimuli-responsive Ca-alginate-based photothermal system with enhanced foliar adhesion for controlled pesticide release. Colloid Surf B. 2021;207:112004. doi:10.1016/j.colsurfb.2021.112004.
19. Liu YY, Huo Y, Li M, Qin CR, Liu HB. Synthesis of metal-organic-frameworks on polydopamine modified cellulose nanofibril hydrogels: constructing versatile vehicles for hydrophobic drug delivery. Cellulose. 2022;29(1):379–93. doi:10.1007/s10570-021-04267-x.
20. Abdalkarim SYH, Yu H, Wang C, Chen Y, Zou Z, Han L, et al. Thermo and light-responsive phase change nanofibers with high energy storage efficiency for energy storage and thermally regulated on-off drug release devices. Chem Eng J. 2019;375:121979. doi:10.1016/j.cej.2019.121979.
21. Qu B, Luo Y. Chitosan-based hydrogel Microspheres: preparations, modifications and applications in food and agriculture sectors—a review. Int J Biol Macromol. 2020;152:437–48. doi:10.1016/j.ijbiomac.2020.02.240.
22. Yang M, Hu J, Meng J, Shan X. A thermo and photoresponsive dual performing hydrogel for multiple controlled release mechanisms. Iran Polym J. 2020;29(10):891–900. doi:10.1007/s13726-020-00846-0.

23. Li L, Qin Y, Wang H, Li M, Song G, Wu Y, et al. Improving thermal conductivity of poly(vinyl alcohol) composites by using functionalized nanodiamond. Compos Commun. 2021;23(4):100596. doi:10.1016/j.coco.2020.100596.
24. Li H, Wang J, Luo Y, Bai B, Cao F. pH-responsive eco-friendly chitosan-chlorella hydrogel microspheres for water retention and controlled release of humic acid. Water. 2022;14(8):1190. doi:10.3390/w14081190.
25. Abdelaty MSA. A facile method for the preparation of hydrophilic-hydrophobic functional thermo-pH responsive terpolymers based on poly (NIPAAm-co-DMAA-co-DMAMVA) and post-polymerization. J Polym Environ. 2021;29(10):3227–41. doi:10.1007/s10924-021-02117-2.
26. Liao Y, Wang M, Chen D. Preparation of polydopamine-modified graphene oxide/chitosan aerogel for Uranium(VI) adsorption. Ind Eng Chem Res. 2018;57(25):8472–83. doi:10.1021/acs.iecr.8b01745.
27. Liu SP, Yu Y, Jiang SS, Li JW, Wang S, Chen SJ, et al. Biocompatible gradient chitosan fibers with controllable swelling and antibacterial properties. Fibers Polym. 2021;23(1):1–9. doi:10.1007/s12221-021-3276-8.
28. Wiwatsamphan P, Chirachanchai S. Persistently reversible pH-/thermo-responsive chitosan/poly(*N*-isopropyl acrylamide) hydrogel through clickable crosslinked interpenetrating network. Polym Degrad Stab. 2022;198:109874. doi:10.1016/j.polymdegradstab.2022.109874.
29. Song R, Zheng J, Liu Y, Tan Y, Yang Z, Song X, et al. A natural cordycepin/chitosan complex hydrogel with outstanding self-healable and wound healing properties. Int J Biol Macromol. 2019;134:91–9. doi:10.1016/j.ijbiomac.2019.04.195.
30. Zheng D, Bai B, He Y, Hu N, Wang H. Synthesis and characterization of dopamine-modified Ca-alginate/poly(*N*-isopropylacrylamide) microspheres for water retention and multi-responsive controlled release of agrochemicals. Int J Biol Macromol. 2020;160:518–30. doi:10.1016/j.ijbiomac.2020.05.234.
31. Lim DG, Kan E, Jeong SH. pH-dependent nanodiamonds enhance the mechanical properties of 3D-printed hyaluronic acid nanocomposite hydrogels. J Nanobiotechnol. 2020;18(1):88. doi:10.21203/rs.3.rs-18085/v1.
32. Chen X, Zhou J, Zhang Y, Zhu S, Tian X, Meng F, et al. Polydopamine-modified polyaniline/nanodiamond ternary hybrids with brain fold-like surface for enhanced dual band electromagnetic absorption. ACS Appl Polym Mater. 2019;1(3):405–13. doi:10.1021/acsapm.8b00127.
33. Zhao H, Wang YT, Zhao S, Fu Y, Zhu L. HOMEOBOX PROTEIN 24 mediates the conversion of indole-3-butyric acid to indole-3-acetic acid to promote root hair elongation. New Phytol. 2021;232(5):2057–70. doi:10.1111/nph.17719.
34. Obireddy SR, Lai W-F. Multi-component hydrogel microspheres incorporated with reduced graphene oxide for pH-responsive and controlled co-delivery of multiple agents. Pharmaceutics. 2021;13(3):313. doi:10.3390/pharmaceutics13030313.
35. Nazlı AB, Açıkel. YS. Loading of cancer drug resveratrol to pH-sensitive, smart, alginate- chitosan hydrogels and investigation of controlled release kinetics. J Drug Deliv Sci Technol. 2019;53:101199. doi:10.1016/j.jddst.2019.101199.